A micromechanical fracture analysis to investigate the effect of healing particles on the overall mechanical response of a self-healing particulate composite

Ponnusami, Sathiskumar A.; Krishnasamy, Jayaprakash; Turteltaub, Sergio; van der Zwaag, Sybrand

DOI
10.1111/ffe.12929

Publication date
2019

Document Version
Final published version

Published in
Fatigue and Fracture of Engineering Materials and Structures

Citation (APA)
Ponnusami, S. A., Krishnasamy, J., Turteltaub, S., & van der Zwaag, S. (2019). A micromechanical fracture analysis to investigate the effect of healing particles on the overall mechanical response of a self-healing particulate composite. *Fatigue and Fracture of Engineering Materials and Structures*, *42*(2), 533-545. https://doi.org/10.1111/ffe.12929

Received: 17 July 2018 | Revised: 28 August 2018 | Accepted: 3 September 2018

DOI: 10.1111/ffe.12929

ORIGINAL CONTRIBUTION

WILEY

A micromechanical fracture analysis to investigate the effect of healing particles on the overall mechanical response of a self-healing particulate composite

Sathiskumar A. Ponnusami[1,2] | Jayaprakash Krishnasamy[1] | Sergio Turteltaub[1] | Sybrand van der Zwaag[1]

[1]Faculty of Aerospace Engineering, Delft University of Technology, Delft, The Netherlands

[2]Solid Mechanics and Materials Engineering, Department of Engineering Science, University of Oxford, Oxford, UK

Correspondence
Sathiskumar A. Ponnusami, Faculty of Aerospace Engineering, Delft University of Technology, Kluyverweg 1, 2629 HS, Delft, The Netherlands.
Email: sathis.ponnusami@eng.ox.ac.uk

Funding information
Dutch Government's IOP Self Healing Materials , Grant/Award Number: SHM01021 ; European Union's seventh framework program (FP7) - NMP SAMBA project , Grant/Award Number: 309849

ABSTRACT

A computational fracture analysis is conducted on a self-healing particulate composite employing a finite element model of an actual microstructure. The key objective is to quantify the effects of the actual morphology and the fracture properties of the healing particles on the overall mechanical behaviour of the ($MoSi_2$) particle-dispersed Yttria Stabilised Zirconia (YSZ) composite. To simulate fracture, a cohesive zone approach is utilised whereby cohesive elements are embedded throughout the finite element mesh allowing for arbitrary crack initiation and propagation in the microstructure. The fracture behaviour in terms of the composite strength and the percentage of fractured particles is reported as a function of the mismatch in fracture properties between the healing particles and the matrix as well as a function of particle/matrix interface strength and fracture energy. The study can be used as a guiding tool for designing an extrinsic self-healing material and understanding the effect of the healing particles on the overall mechanical properties of the material.

KEYWORDS
cohesive elements, fracture mechanism, fracture properties, healing particles, self-healing material, thermal barrier coatings

1 | INTRODUCTION

Self-healing materials can be classified into two broad classes, extrinsic and intrinsic, depending upon the healing mechanism and the healing agent involved. In an intrinsic self-healing material, the healing agent is contained within the host material as its integral constituent. In other words, the healing action is due to the physiochemical nature of the material itself.[1] When damage or cracking occurs, one or more constituents of the material act as the healing agent, which upon completion of the healing process aid in the recovery of the mechanical properties. Such intrinsic self-healing mechanisms can be found in several material classes that include ceramics,[2,3] cementitious materials,[4] and polymers.[5] In the second class of self-healing materials, the extrinsic ones, the healing agent is not part of the original material itself, rather a discrete foreign material constituent is added to the host material during the fabrication process.[6-11] This class has been a popular approach in the early stages of the field of self-healing materials development as it favours incor-

porating healing mechanism into any class of material system that does not inherently possess a self-healing characteristic. One of the widely used techniques under this category is encapsulation of the healing agent and dispersing the healing capsules within the host material. When a crack appears in such a material, it interacts with the healing capsule, followed by its rupture or fracturing.[12-15] Upon opening of the capsule, the healing agent flows or diffuses into the crack eventually leading to crack filling. Such a healing process involves a sequence of steps starting from crack-capsule interaction, rupture of the capsule, followed by the release of the healing agent into the crack, and finally formation of the healing product through a chemical or a physical reaction. The resulting healing product, in turn, binds the crack faces together and restores the mechanical integrity of the material.

From the perspective of (extrinsic) self-healing material design, the properties of the healing particles in relation to the host matrix are very crucial for successful realisation of a self-healing material system. In particular, for the selection and design of healing capsules, the following two requirements have to be met to result in an ideal self-healing material design:

- In order to enable activation of the healing process, the microcracks in the matrix material should get attracted towards the healing particles and break them, instead of deflecting away from the particles that would prevent healing activation.
- The introduction of healing particles into the matrix should not deteriorate the mechanical properties of the host matrix material. In other words, the structural integrity of the material should not be compromised with the dispersion of the healing particles.

The above two requirements are often contradictory as promoting particle fracture for healing is likely to degrade the composite strength, in general. Hence, for an optimal design of the self-healing material, a balance between these two requirements has to be achieved. This, in turn, lies in a careful selection and design of the healing particles in terms of their geometric and material properties and their spatial distribution. The first requirement is dealt in detail,[16] whereby fracture maps distinguishing the fracture mechanisms are generated through extensive two-dimensional analyses on a single-particle matrix system. In this current work, the primary objective is to address the second requirement, whereby microstructure-based two-dimensional finite element fracture simulations are conducted for the quantification of the effect of healing capsules on the mechanical properties.

Microstructure-based finite element simulations have been conducted in the literature to analyse fracture and damage in particulate composite systems.[17-25] For examples, microstructures representing a random distribution of irregularly shaped SiC particles in an aluminum matrix were simulated using two-dimensional linear elastic approach involving stress intensity factor as the crack driving force parameter.[17,18] The effect of particle clustering was quantified, and the resulting crack paths were compared with experiments. In a different work,[19] an actual microstructure of a particulate composite was modelled by mapping the scanning electron microscope (SEM) images onto the finite element mesh. They investigated the effects of pore defects and residual stresses on the crack path by employing Griffith energy-based fracture mechanics approach. An elastoplastic finite element analysis was conducted on an SEM-based finite element model, and the stress-strain response was reported as a function of microstructural features such as particle clustering.[20] A comprehensive investigation of the effect of distribution, size, and shape of the particulate reinforcements and interphase properties on the fracture behaviour of a Al_2O_3/TiB_2 composite has been conducted.[23,24] Employing a J-integral concept and using a cohesive zone approach to simulate fracture in the matrix, the particle, or the interface, the effective fracture toughness of the composite was quantified. The abovementioned analyses were performed in a two-dimensional framework. Some efforts have been taken to conduct three-dimensional crack propagation analysis in particulate composites,[26-28] but the computational cost associated with such simulations limits the scope of such studies in terms of number of particles that can be analysed. Further, the computational intensity prevents the possibility of conducting a series of parametric analysis to explore the effect of microstructural features and the influence of constituent properties.

In the context of self-healing particulate composite systems, a limited number of modelling studies have been conducted in terms of quantifying the effective mechanical properties and crack path predictions.[28-33] For instance, efforts are taken to estimate the effective elastic properties of self-healing particulate composites, whereby the effect of dispersed healing particles on the elastic moduli of the host matrix material is quantified.[30,31] Crack propagation studies were conducted in an idealised healing capsule(s)-matrix system, and the effects of geometric and material parameters were analysed using cohesive zone model and extended finite element method (XFEM).[28] In particular, a self-healing concrete in a three-point bending test set-up was utilised to evaluate the influence of parameters such as number, size, and position of capsules on the mechanical behaviour of the concrete. This was then followed by modelling an idealised single healing

capsule-matrix volume element, whereby the influence of interface properties and capsule volume fraction on the effective strength was reported. Nonetheless, for further material development, it is important to determine the expected performance under actual conditions. Correspondingly, the objective of the present research is to study the crack propagation in a real microstructure of a self-healing particulate composite, followed by the quantification of the effect of the healing particles and their properties on the composite mechanical behaviour. This is achieved through numerical analysis using a finite element model generated directly from an actual microstructure of the $MoSi_2$-YSZ composite.[34] The motivation is to reveal the roles of these parameters to experimental researchers, which could be helpful in the design and development of self-healing systems with least compromised mechanical property values of the original intact base material.

2 | MICROSTRUCTURE AND MODELLING APPROACH

An actual composite microstructure is shown in Figure 1 where the $MoSi_2$ particles, which is the discontinuous phase, are randomly dispersed in the YSZ matrix. The nominal volume fraction of the $MoSi_2$ particles is 20%. Additional information of the composite material such as manufacturing process and details of the material constituents of the composite can be found elsewhere.[34] The geometry of the microstructure shown in Figure 1 was generated through postprocessing of an SEM image of the composite cross-section, which is then translated into a finite element mesh; see right side of Figure 1 showing a part of the mesh. A small initial precrack of length equal to 0.025 mm was included on the left side of the composite specimen. The length and the width of the model are equal to 0.7 mm and 0.4 mm, respectively.

In the present work, cohesive elements are employed for analysing fracture in the particle/matrix system, whose behaviour is governed by the bilinear traction-separation law.[35] The microstructure is meshed using two-dimensional three-node plane-strain elements (CPE3) for the particle and the matrix phases, to model their bulk constitutive behaviour. In order to simulate fracture, the initial finite element mesh was modified using a Matlab pre-processing script to include four node cohesive elements (COH2D4) throughout all the interelement boundaries in the finite element mesh. This process of embedding cohesive elements throughout the mesh introduces potential crack faces necessary to simulate all the relevant fracture mechanisms such as interface debonding, particle fracture, and matrix cracking. However, such an approach naturally triggers the issue of mesh dependency in terms of the artificial compliance and the converged crack path. This aspect has been taken into consideration and subsequently resolved using the guidelines derived from the mesh dependency study.[16] The resulting finite element mesh consists of about 10^6 elements, of which approximately 60% are cohesive elements and the remaining 40% are plane-strain bulk elements. For the bulk elements in the particle and the matrix phases, a linear elastic and isotropic constitutive behaviour is assumed. For the cohesive elements, the bilinear cohesive relation (described below) is utilised, through which corresponding fracture properties (strength and fracture energy) are assigned for failure modelling in the particle, the matrix, and the particle/matrix interface.

Note that the microstructure considered in the analysis is a cross-section of the particulate composite. Hence, the two-dimensional finite element model of the microstructure does not entirely reproduce the microstructural

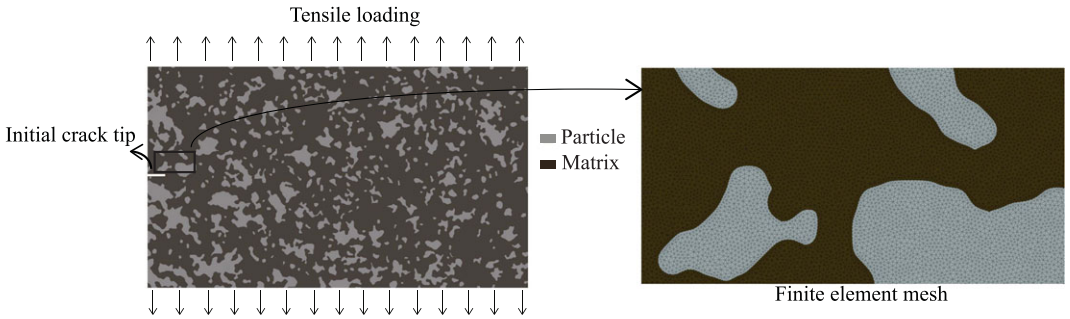

FIGURE 1 Microstructure and loading conditions of a self-healing particle-matrix composite system. Finite element mesh was generated after processing an SEM picture of ($MoSi_2$) particles (lighter phase) embedded in yttria stabilised zirconia (YSZ, darker phase). A part of the finite element mesh is shown on the right. Cohesive elements of zero geometric thickness were embedded along all interelement boundaries in the finite element mesh. A small initial precrack of length equal to 0.025 mm, schematically highlighted as a notch for better clarity, was included on the left side of the model. The length and the width of the specimen are equal to 0.7 mm and 0.4 mm, respectively [Colour figure can be viewed at wileyonlinelibrary.com]

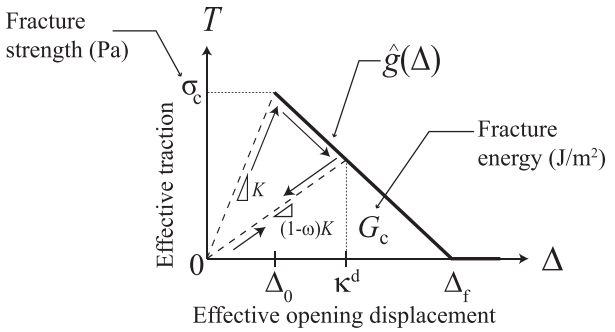

FIGURE 2 A bilinear traction-separation law, ie, with linear softening. The arrows show steps such as loading, damage, unloading, and reloading

features as the three-dimensionality is naturally lost in the model. As a matter of fact, the finite element model assumes that the cross-section of the particles is extruded in the third direction representing cylindrical inclusions rather than the actual particles. Despite these limitations, the microstructure-based fracture analysis in a two-dimensional framework is undertaken to reveal qualitative and some quantitative information in terms of the fracture mechanisms and the mechanical properties of the composites. Two-dimensional fracture analyses can be effectively used as a pragmatic approach to understand the effect of properties of the constituents (particle, matrix, and interface) on the crack path, a crucial information for self-healing material design.

For completeness and in order to introduce the required notation, the cohesive zone model used in the present analysis is briefly summarised below.[16,35,36] The cohesive law illustrated in Figure 2 corresponds to a bilinear relation between T, which is a scalar measure of the traction $\boldsymbol{t}$ transmitted across the cohesive surface, and Δ, which is a scalar measure of the cohesive surface opening displacement vector $\boldsymbol{\delta}$. The traction T increases with increasing cohesive surface opening displacement Δ up to a maximum value given by the material fracture strength, σ_c, and eventually decreases linearly to zero, at which point the cohesive zone is fully separated. The area under the traction-separation curve, which represents the total work per unit area expended in creating a fully separated crack, corresponds to the fracture energy G_c of the material.

The traction-separation law relates the traction $\boldsymbol{t}$ acting on the crack faces, with components (t_n, t_s), to the crack opening vector $\boldsymbol{\delta}$, with components (δ_n, δ_s), where the subscripts "n" and "s" refer to the directions normal and tangential to the crack face, respectively. An effective crack opening Δ can be defined as

$$\Delta := \sqrt{\langle \delta_n \rangle^2 + \gamma^2 \delta_s^2}, \tag{1}$$

where $\langle \cdot \rangle = (\cdot + |\cdot|)/2$ refers to the Macaulay bracket and γ is a non-dimensional mixed-mode parameter assigning weights for the modes I and II contributions, which is defined as

$$\gamma = \frac{\delta_{n,0}}{\delta_{s,0}} \quad ,$$

where $\delta_{n,0}$ and $\delta_{s,0}$ denote, respectively, the crack opening at the onset of failure for pure Mode-I and pure Mode-II. Denoting by $t_{n,c}$ and $t_{s,c}$ the corresponding values of the normal and tangential cohesive strength, then $t_{n,c} = K\delta_{n,0}$ and $t_{s,c} = \gamma^2 K \delta_{s,0}$. This will yield $\Delta_0 = \delta_{n,0} = \gamma \delta_{s,0}$, and using the stiffnesses K and $\gamma^2 K$ in modes I and II, respectively, then $\sigma_c = t_{n,c} = t_{s,c}/\gamma$. Complete loss of cohesion occurs for pure modes I and II, respectively, at $\delta_{n,f}$ and $\delta_{s,f}$, with $\Delta_f = \delta_{n,f} = \gamma \delta_{s,f}$.

In order to determine whether the crack opening is increasing or decreasing due to the external loading process, the following loading function f^d is used:

$$f^d = \hat{f}^d(\Delta, \kappa^d) := \Delta - \kappa^d, \tag{2}$$

where $\kappa^d = \kappa^d(t)$ is a damage history variable that, at a given time t, corresponds to the maximum value attained by the equivalent crack opening during a process up to that time. The loading and unloading conditions correspond to the Karush-Kuhn-Tucker relations; see Figure 2.

The equivalent crack opening Δ is used to compute the equivalent traction T as

$$T = \hat{T}(\Delta, \kappa^d) = \begin{cases} \hat{g}(\Delta) & \text{if} \quad f^d = 0 \text{ and } \dot{\kappa^d} > 0, \\ \hat{g}(\kappa^d)\frac{\Delta}{\kappa^d} & \text{otherwise,} \end{cases} \tag{3}$$

where $\hat{g}$ is the effective traction-separation law and $\dot{\kappa}^d$ indicates the (time) rate of change of the damage history variable. The upper and lower expressions in (3) provide the equivalent traction during, respectively, crack growth and unloading/reloading. Alternatively, one could work with a damage variable ω and consider a "damaged" stiffness such that $(1-\omega)K = \hat{g}(\kappa^d)/\kappa^d$ as indicated in Figure 2. The specific form of the effective traction-separation law used in the present work is a linear softening relation (see Figure 2), which corresponds to

$$g = \hat{g}(\Delta) = \sigma_c \frac{\langle \Delta_f - \Delta \rangle}{\Delta_f - \Delta_0}. \tag{4}$$

The initially linearly "elastic" loading up to the fracture strength in a bilinear law can be reproduced in Equation 3 by assigning an initial damage $\kappa^d(0) = \kappa_0^d = \Delta_0$. The parameter Δ_f is chosen such that the integral of $\hat{T}$ from $\Delta = 0$ to $\Delta = \Delta_f$ equals the material fracture energy G_c, i.e., $\Delta_f = 2G_c/\sigma_c$.

After evaluating Equation 3, the normal and shear tractions can be computed as

$$t_n = \begin{cases} \frac{\delta_n}{\Delta} T & \text{if} \quad \delta_n > 0, \\ K\delta_n & \text{if} \quad \delta_n < 0, \end{cases} \qquad t_s = \gamma^2 \frac{\delta_s}{\Delta} T, \tag{5}$$

ie, for $\delta_n \geq 0$, one has that $\boldsymbol{t} \cdot \boldsymbol{\delta} = T\Delta$.

The finite element model is subjected to a global Mode-I loading by prescribing displacements on the upper and lower edges of the specimen, which contains a small edge precrack on the left as shown in the Figure 1. With reference to the literature,[37,38] the elastic properties used for the particle and the matrix are as follows: Young modulus of the YSZ matrix is taken as $E^m = 150$ GPa and that of the $MoSi_2$ particle is given as $E^p = 450$ GPa. Poisson's ratio of the particle and the matrix are kept equal to 0.25. In the related literature, a significant scatter was observed in the strength and the fracture energy of the matrix and the particle and they depend on various factors such as temperature, manufacturing technique, and chemical composition.[39-42] So, in the current study, a parametric approach is taken, whereby a range of relative fracture properties are considered and their effects on the crack path and the composite properties are quantified. The strength and the fracture energy of the matrix are taken, respectively, as $\sigma_c^m = 300$ MPa and $G_c^m = 0.1$ N/mm, whereas the strength and fracture energy of the particle and the interface (σ_c^p, G_c^p, σ_c^i, G_c^i) are varied with respect to the corresponding matrix properties for the analyses. The details on the fracture properties of the particle and the interface and their variations are specified in the relevant sections. All the analyses were conducted in Abaqus using implicit Newton-Raphson iterative solver. A sufficiently small value of viscosity equal to 1.0×10^{-6} is used in the analysis to deal with convergence difficulties encountered during the simulations, which involved multiple cracking and coalescence in several cases.

The approach of the study is to conduct a series of parametric studies and to derive the composite specimen strength from the resulting load-displacement responses. It is to be noted that the term specimen (average) strength is used instead of effective strength, as the objective is not to derive homogenised composite properties, rather to reveal the role of fracture property mismatch on the global mechanical behaviour. The term "average" represents the normalisation of the load by the area over which the load is applied and the displacement by the corresponding length in the loading direction for the stress and the strain, respectively. However, the specimen properties obtained from the analysis would become the effective properties of the composite if appropriate measures are taken while applying the boundary conditions and if the specimen size is ensured to be sufficiently large to be considered as a representative volume element (RVE). For convenience, the average specimen stress and the strain in the composite are denoted by σ^c and ε^c, respectively. The results obtained from this study are presented in terms of normalised values of the above measures with respect to the corresponding values of the homogeneous (matrix) specimen.

In the next two sections, the effect of fracture properties of the particle and the interface on the composite properties is investigated, for which a stiffer particle case is considered, by fixing the modulus mismatch ratio as $E^p/E^m = 3$, in accordance with the particulate composite considered for the self-healing TBC.

3 | EFFECT OF PARTICLE FRACTURE PROPERTIES ON MECHANICAL BEHAVIOUR

The influence of the fracture properties of the particles on the specimen strength is analysed in this section. The variations in the crack path are reported for two representative cases, one corresponding to weaker particles and the second corresponding to stronger particles reinforced in the matrix material. Subsequently, a range of fracture properties (strength and energy) of the particles is considered to study its effect on the mechanical response of the composite.

3.1 | Crack trajectory for particles of different strengths

3.1.1 | Weaker particle case

A simulation is carried out with the properties mentioned in Section 2 for the particle and the matrix, except that the strength of the particle is reduced by 25% with respect to the matrix, resulting in a strength mismatch ratio, $\sigma_c^p/\sigma_c^m = 0.75$ between the particle and the matrix. The fracture energy of the particle and the matrix are kept the same and equal to 0.1 N/mm. The particle is assumed to be perfectly bonded to the matrix, which is achieved by assigning a very high fracture strength for the interface with respect to the properties of the particle and the matrix. The simulated crack path through the microstructure is shown in Figure 3 (indicated in white). It can be observed that the propagating crack finds the weaker path by fracturing all the particles that are in the neighbourhood of the advancing crack tip. In this case, particles fracture despite the fact that the healing particles are stiffer than the matrix by a factor of 3. Thus, the mismatch in the fracture strength (making the particle weaker) has a stronger effect in deciding the crack path when compared with the effect of the mismatch in elastic properties. This result is relevant for

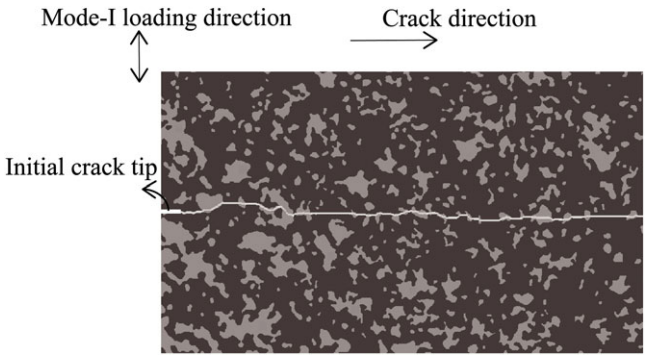

FIGURE 3 Simulated crack growth on a particle/matrix system with relatively weak particles given by the strength mismatch, $\sigma_c^p/\sigma_c^m = 0.75$ between the particle and the matrix (propagating crack path is from left to right). Perfect particle/matrix bonding is assumed in this simulation. A stiffer particle case is considered given by the elastic mismatch ratio, $E^p/E^m = 3$, between the particle and the matrix. The fracture energy of the particle, the matrix, and the interface are kept equal to 0.1 N/mm [Colour figure can be viewed at wileyonlinelibrary.com]

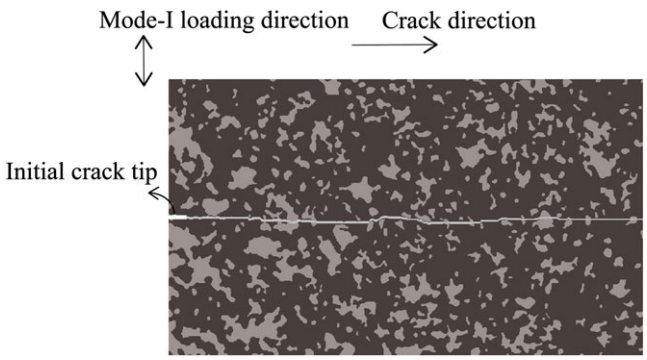

FIGURE 4 Simulated crack growth on a particle/matrix system with relatively strong particles given by the strength mismatch, $\sigma_c^p/\sigma_c^m = 1.25$ (propagating crack path is from left to right). Perfect particle/matrix bonding is assumed in this simulation. Fracture energies of all the phases are kept the same and equal to 0.1 N/mm [Colour figure can be viewed at wileyonlinelibrary.com]

a capsule-based self-healing mechanism since it indicates that healing activation can be achieved even if the particles are relatively stiffer than the matrix and crack-particle interaction is in principle deflective.

3.1.2 | Strong particle case

The second case of interest is the situation when the strength of the particle is higher than that of the matrix. In this section, the simulation is performed with the material properties indicated in Section 2, except that the strength of the particle is increased by 25% as compared with the matrix strength, which corresponds to a particle strength mismatch ratio, $\sigma_c^p/\sigma_c^m = 1.25$. The fracture energy of the particle and the matrix are kept the same and equal to 0.1 N/mm. Again, the bonding between the particle and the matrix is assumed to be perfect. The resulting crack path is reported in Figure 4 (indicated in white). From the simulated crack path, it can be observed that the crack propagates preferentially through the matrix, thus, in general, avoiding the particles. However, on a few occasions, particle fracture did occur, when the particle is directly in front of the approaching crack. A similar observation has been made in the literature.[23] Such instances of particle fracture despite its higher strength can also be attributed to the irregular shape and clustering of the particles (ie, local stress conditions occur such that particle fracture is favoured). Furthermore, in these particular cases, prevention of particle fracture would require an unrealistic deflection of the crack tip. As a general conclusion, a composite with particles of higher strength precludes fracturing of the particles. Such a scenario is unfavourable from a self-healing materials design viewpoint as this fracture mechanism would prevent triggering of the healing mechanism.

3.2 | Effect on composite strength

To analyse the effect of the fracture properties of the particles on the composite strength, a range of values of particle strength ratios are considered, given by $\sigma_c^p/\sigma_c^m = 0.05$, 0.25, 0.33, 0.5, 0.75, 1, and 1.25. For each of the above strength ratios, three different fracture energy ratios of the particles with respect to the matrix fracture energy are considered and are given by G_c^p/G_c^m=1/5, 1, and 5. The results of the simulations are summarised in Figures 5 and 6. Figure 5 shows the average stress-strain responses for some selected strength ratios, which provide the insights into the response history of the composite. Some important observations can be made from the plot. Firstly, the strength of the composite specimen decreases with decrease in the particle strength. The strain corresponding to the peak stress (or strength) in the stress-strain curve decreases with decrease in the particle strength. It can also be noted that the point at which the curves deviate from the elastic response decreases as the strength decreases. This is an indication of the onset of damage prior to the peak load.

To summarise the results of all the simulations for varying particle strength and fracture energy, Figure 6A shows the variation of the resulting strength of the composite specimen with respect to the particle fracture properties (strength and energy). As discussed before, the results clearly show a strong influence of the particle fracture properties on the mechanical response of the composite specimen. From the plot shown in Figure 6A, it can be observed that decreasing the strength of the particle in relation to the matrix strength severely decreases the composite strength. For instance, the strength of the composite is decreased by 25% with respect to the reference

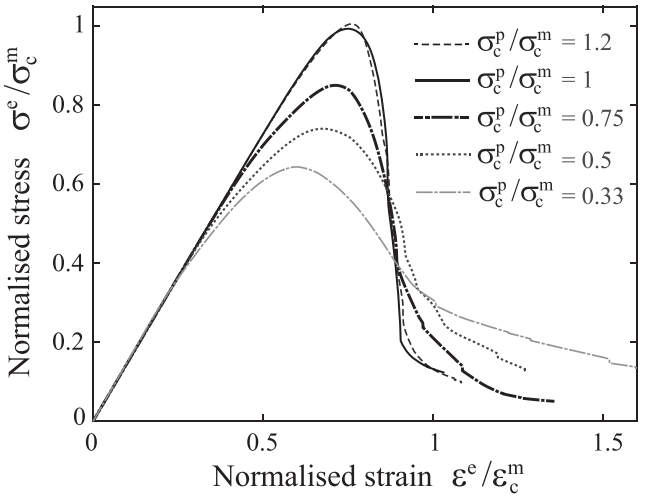

FIGURE 5 Effect of particle strength on the normalised stress-strain response of the composite specimen. The fracture energy of the particle and the matrix are kept the same. Perfect interface bonding is considered

homogeneous matrix specimen strength, when the particle strength is reduced by 50%. On the other hand, increasing the particle strength above the matrix strength does not improve the strength of the composite as observed from the results. On the effect of fracture energy, a similar effect is i.e., decreasing the fracture energy of the particle reduces the composite strength as shown in Figure 6A. However, it has to be noticed that the effect of fracture energy ratio is pronounced only in the intermediate ranges of the strength ratios. In other words, when the particle strength is higher than that of the matrix or very low, then the composite strength is insensitive to the fracture energy of the particle as observed from the Figure 6A.

3.3 | Instances of particle fracture

A parameter of interest for a particle-based self-healing mechanism is the percentage of fractured particles, p which is defined as $n/\mathrm{N} \times 100$, where n is number of the fractured particles in the simulated crack path and N is the number of particles encountered or traversed by a crack if the crack path were a perfect straight line originating from the initial crack tip. Through postprocessing of the fractured microstructures for various particle properties, the percentage of fractured particles is determined and plotted as the function of the fracture properties of the particles in Figure 6B. As a general observation, decreasing the strength of the particle favours particle fracture as observed from Figure 6B, a requirement for healing activation. However, the maximum number of fractured particles saturates when the particle strength is reduced below the strength ratio, $\sigma_c^p/\sigma_c^m = 0.6$, and is around 160%. This indicates that the crack traverses the material preferentially through particles located above and below an ideal straight path. On the lower side, the percentage of fractured particles reduces to just 10% if the particle strength ratio is increased to a value beyond $\sigma_c^p/\sigma_c^m = 1$. The fracture mechanism is very sensitive to the mismatch in the strength of the particle especially when the particle strength ratio is perturbed around the value of one.

When it comes to the fracture energy mismatch, the effect is less pronounced as compared with the strength ratio, which is consistent with the observations reported in the previous work of the authors.[16] Increasing the fracture energy does not reduce the percentage of fractured particles significantly, although reducing the fracture energy of the particle has a more pronounced effect as observed from Figure 6B.

The two plots showing the variation of the composite strength and the percentage of fractured particles, with respect to particle fracture properties provide an insight on how to achieve a balance between the two contradictory requirements for self-healing material design. For instance, the objective of particle fracture (or healing activation) can be achieved with healing particles that are only slightly weaker than the matrix. For example, for the strength ratio, $\sigma_c^p/\sigma_c^m = 0.833$, a high percentage of fractured particles can be realised with just 5% reduction in composite strength; see Figure 6B. Thus, if the healing particles can be engineered such that their strength is slightly lower than the matrix strength, a successful self-healing system can be achieved in terms of healing activation without significantly compromising the fracture properties of the composite.

4 | EFFECT OF INTERFACE FRACTURE PROPERTIES ON MECHANICAL BEHAVIOUR

Another important feature that governs the global mechanical behaviour of the particulate composite is the interface between the particle and the matrix. In the context of self-healing materials, the requirement on the interface properties is not straightforward. An ideal combination for a robust self-healing system would be a relatively weaker particle perfectly bonded to the surrounding matrix material. In that case, high interface strength is advantageous for efficient load transfer, whereby both the particles and the matrix are load-bearing constituents in the composite. However, if the particle is stronger than the matrix, particle fracture is less likely to occur, which, in turn, does not activate the healing mechanism when required. In such scenario, a relatively weaker interface could help in facilitating debonding between the particle and the matrix and expose the heal-

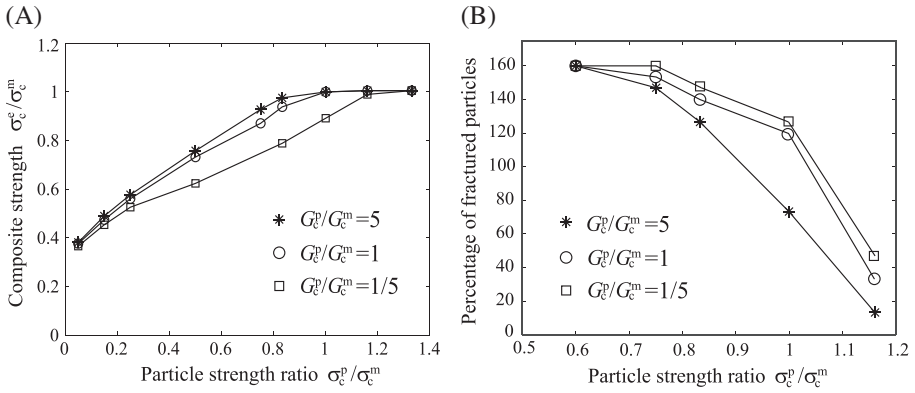

FIGURE 6 Effect of particle fracture properties on the composite strength and the percentage of fractured particles. The particle strength is varied over a range, whereas for the particle fracture energy, three different ratios are considered as shown in the plots. A, Variation of composite strength vs particle fracture properties. B, Normalised percentage of fractured particles vs particle fracture properties

ing particle to the crack. It is important to emphasise that the term "interface" used here refers to a discrete zero thickness layer between the particle and matrix with its own fracture properties. In some practical cases, encapsulation of healing particles are done leading to a thin third phase (interphase) layer between the particle and the interface.[14,43] In such cases, the results obtained from the current study should be interpreted in the context that the failure of the interface would mean the failure of the encapsulating interphase layer.

To investigate the role of interface fracture properties, a series of simulations are conducted for varying interface fracture properties, while fixing the stiffness mismatch ratio between the particle and the matrix, given by $E^p/E^m = 3$. The strength and fracture energy of the particle and the matrix are kept the same and are given by $\sigma_c^p = \sigma_c^m = 300$ MPa and $G_c^p = G_c^m = 0.1$ N/mm, respectively. Firstly, the crack path corresponding to a representative system with a weak interface strength is discussed, followed by detailed quantification of effect of the interface properties on the mechanical response.

4.1 | Crack trajectory for an interface of low bond strength

The crack path resulting from the simulation with an interface strength mismatch ratio, $\sigma_c^i/\sigma_c^m = 0.75$, is shown in Figure 7. It can be observed that the crack predominantly deflects its path towards the particle/matrix interfaces. Crack advancement occurs primarily through debonding along the interfaces between the particles and the matrix. Nevertheless, at few instances, it is observed that particle fracture occurs when the particle is directly in front of the approaching crack or when it is relatively larger in size, making it difficult for the crack to circumvent the interface. From the perspective of successfully triggering the

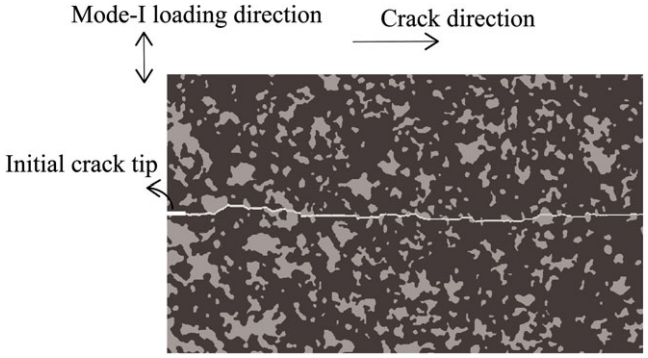

FIGURE 7 Simulated crack growth on a particle/matrix system with relatively weak interface given by the strength mismatch, $\sigma_c^i/\sigma_c^m = 0.75$ between the interface and the matrix (propagating crack path is from left to right). The fracture energy of all the phases are kept equal to 0.1 N/mm. The strength of the particle and the matrix are kept equal [Colour figure can be viewed at wileyonlinelibrary.com]

healing mechanism, a weaker interface is in general not preferable as it does not necessarily lead to particle fracture. However, interface debonding could be considered as the second favourable fracture mechanism after particle fracture, as the probability of exposing the healing agent contained within the particle to the crack is likely to be high, potentially leading to healing activation.

4.2 | Effect on composite strength

For detailed quantification of interface effects on the mechanical behaviour, the average stress-strain responses of the specimen with four different values for the interface fracture strength, $\sigma_c^i/\sigma_c^m = 0.01, 0.25, 0.5$ and 1 are reported in Figure 8. From the figure, it can be seen that an interface that is perfectly bonded (or at least having equal fracture properties as that of the matrix and the particle) results in a higher overall strength of the speci-

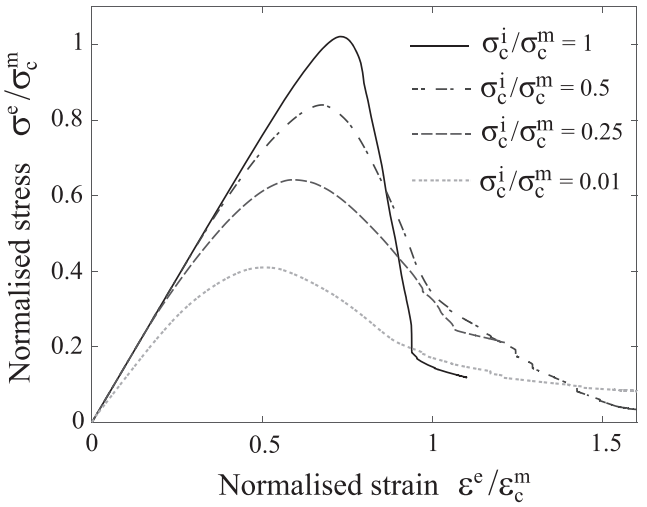

FIGURE 8 Effect of interface strength on the normalised stress-strain response of the composite specimen. The stiffness mismatch ratio is $E^p/E^m = 3$ that corresponds to a stiffer particle. Fracture strength of the matrix and the particle are kept the same. The interface fracture energy is fixed and equal to that of the fracture energy of the particle and the matrix, $G_c^i = G_c^p = G_c^m = 0.1$ N/mm

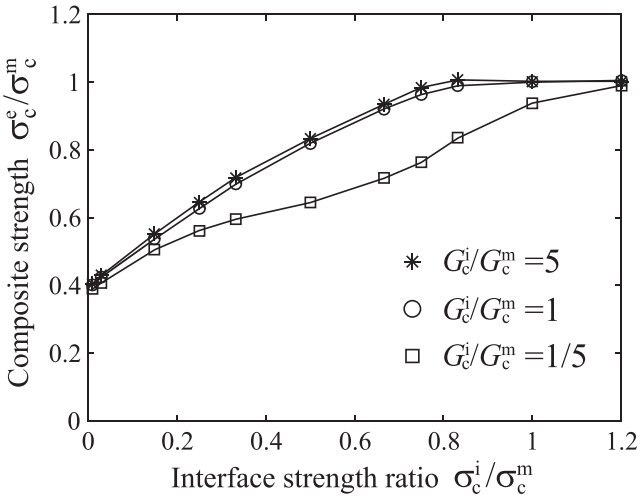

FIGURE 9 Effect of interface strength and fracture energy on strength of the composite specimen. The stiffness mismatch ratio is $E^p/E^m = 3$ that corresponds to a stiffer particle. Fracture properties of the matrix and the particle are kept the same

men as compared with the other responses corresponding to lower interface strengths. This is an expected outcome as stronger interface leads to better load transfer between the matrix and the particle, resulting in higher strength. However, it is worth noting that higher interface strength or perfect bonding leads to a relatively brittle response in the considered set-up. As the interface becomes weaker, interface debonding is preferentially activated and introduces an additional energy dissipating mechanism. This, in turn, leads to enhanced energy dissipation and "ductile" behaviour of the composite, albeit with a reduced composite strength. Such a scenario is often useful in composite materials with brittle-brittle phases whereby engineering the interface aids in introducing ductility in the composite material.[44] The term "ductility" is used in a general sense implying a non-abrupt fracture process and does not mean any plastic deformation. In the present context, it can be quantified as the ratio between the fracture strength and the fracture energy.

The results of several simulations are summarised in Figure 8 in terms of the normalised stress as a function of the strain for various values of the interface strength and in Figure 9 in terms of the composite strength as a function of interface strength and fracture energy. A clear trend is observed revealing the improvement of the composite strength with increase in the interface strength. The strength of the composite specimen saturates when the interface fracture strength is increased beyond the strength of the particle and the matrix, as seen from the plateau region of the curve in Figure 9 for $\sigma_c^i/\sigma_c^m \geq 1$. On the other end, when the interface strength ratio is reduced to a value equal to 0.01 (interface strength is 100 times lower than that of the matrix and particle), the value of the composite specimen strength reaches a lower limit approximately equal to 40% of the homogeneous matrix strength. This can be viewed as the strength of the composite with particles replaced by loose particles (or pores in the limit case) as the interface hardly plays any role in load transfer between the particle and the matrix. Such an explanation is applicable and valid only for tensile strength, but for the same composite under compression, the completely debonded particles would still contribute significantly to the load carrying capability through contact and frictional forces. On the effect of interface fracture energy, increasing the fracture energy of the interface by a factor of 5 does not significantly influence the strength of the composite, but decreasing the interface fracture energy by a factor of 5 reduces the composite strength as observed in Figure 9, which is a similar trend as seen in the effect of particle fracture energy in the previous section.

4.3 | Effect of mode-mixity on composite strength

While analysing fracture in composite materials (particulate or fibre-reinforced), mixed-mode fracture is a common phenomenon occurring in the failure of such materials. Mixed-mode fracture arises from two main sources, one being the applied boundary or loading conditions in such a way that fracture evolves under globally applied mixed-mode loads. The second source is the inherent heterogeneity of the material microstructure that leads to local mixed-mode fracture conditions in the vicinity of

the interfaces between the particles (or fibres) and matrix. This is often the case in composite materials, whereby even when the structure or the composite material is subjected to global Mode-I loading conditions, local stress fields in the crack vicinity are influenced by the presence of particles or fibres (and their interfaces), resulting in crack evolution under mixed-mode conditions. For many materials, the fracture properties are different for different modes of fracture (normal and tangential). More importantly, the fracture properties of an interface between two material phases are found to be significantly different in opening (normal) and shearing (tangential) modes of fracture. Thus, it becomes a natural problem of significance to address the effect of varying interface fracture properties in normal and tangential modes on the mechanical behaviour of the composite material.

In this subsection, fracture analyses are conducted considering different values of the interface strength in Mode-I and Mode-II (normal and tangential strengths), and the effects are quantified in terms of the resulting composite strength. To this end, three sets of analysis are conducted to address the above problem. Firstly, the interface fracture strength (and the energy) is kept the same in both modes ($\gamma = 1$). In the second set of analyses, the interface strength in Mode-II is taken equal to 10 times higher than the strength in Mode-I ($\gamma = 10$, Mode-I dominated fracture). In the third set, the interface shear strength is reduced by a factor of 5 as compared with its normal strength ($\gamma = 1/5$), enabling us to model an interface, which would easily yield to local Mode-II deformation field. In all the three sets, the interface normal strength is varied over a wide range, and the shear strength varies accordingly in the three different sets of analyses described above.

The results of the simulations are obtained in terms of the effective composite specimen response. The results are summarised in Figure 10 in terms of the normalised composite strength as a function of the interface strength ratio, σ_c^i/σ_c^m, for three different values of mixed-mode parameter, γ. The ratio of the interface shear strength to the normal strength of the interface is specified by the mix mode parameter γ. From the results, it can be generally observed that increasing the shear strength of the interface with respect to its normal strength (ie, with increase in γ) increases the resulting composite strength. For the mixed-mode parameter γ equal to 10 (higher shear strength), the composite strength is increased by approximately 8% with respect to the baseline case ($\gamma = 1$) for most of the considered interface strength ratios. However, once the interface (normal) strength is increased beyond the matrix strength, the interface mixed-mode parameter does not influence the composite strength. This is because the interface debonding is automatically arrested when the interface (normal) strength is higher than the matrix (and particle) strength. Any further increase in shear strength of the interface with respect to its normal strength will not affect the strength of the composite.

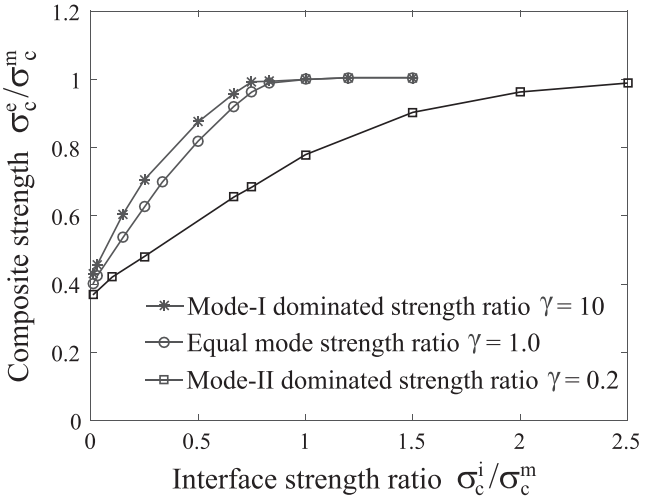

FIGURE 10 Effect of interface mixed-mode strength ratio on strength of the composite specimen. Fracture properties of the matrix and the particle are kept the same. The interface fracture energies are kept equal to that of the fracture energy of the particle and the matrix, $G_c^i = G_c^p = G_c^m = 0.1$ N/mm

On the other hand, for the mixed-mode parameter of the interface equal to 0.2 (lower shear strength), the influence on the composite strength is very strong as observed from Figure 10. The resulting composite strength is drastically reduced as compared with the strength in Mode-I dominated case. This shows that though the prescribed boundary condition is globally Mode-I loading, local mixed-mode effects can play a significant role, especially if the strength of the interface is different in normal and shear modes. In particular, the strength of the composite under Mode-I loading is reduced by 30% for some of the interface (normal) strength ratios considered. Further, in the mixed-mode case with $\gamma = 0.2$, the reduced shear strength of interface affects the composite strength even after the ratio of the interface strength ratio, σ_c^i/σ_c^m, is increased beyond 1. From Figure 10, it can be observed that saturation of the resulting composite strength occurs only when the interface strength ratio is increased to 2.5 (or even above). Thus, the The mixed-mode fracture properties can become important for composite behaviour especially if the fracture properties are significantly different in normal and tangential modes despite the loading conditions being pure Mode-I or Mode-II.

5 | SUMMARY AND CONCLUSIONS

In this study, micromechanical fracture simulations were conducted taking a real $MoSi_2$ particle-filled TBC matrix

microstructure. The results obtained from the analyses reveal that the mismatch in fracture properties of the particle, the matrix, and the interface has a significant influence on the resulting crack path and the mechanical properties. From a self-healing viewpoint, the properties of the healing particle and the interface can be tailored to achieve the healing activation; however, on the other hand, such an approach affects the overall macroscopic strength of the resulting composite, which becomes detrimental to the material system. Care must be taken in order to achieve a trade-off between the resulting initial composite properties and the healing activation as it is natural that both the requirements could be contradicting in many practical self-healing materials. From the extensive fracture analyses on the composite microstructure, the following conclusions were arrived at:

- The mechanical properties of the composite (the strength) are significantly influenced by the fracture properties of the particle. The effect of the particle strength is more pronounced than that of its fracture energy in determining the composite properties.
- The percentage of fractured particles in the resulting crack path is very sensitive to the fracture strength of the particle. Particles that are slightly weaker than the matrix can trigger particle fracture (hence the healing mechanism), importantly without compromising the composite properties noticeably.
- Interface fracture properties have a dominant effect on the composite properties. In case of interface-dominated fracture, mixed-mode fracture properties of the interface play a crucial role on the resulting composite strength.

The results and conclusions from the microstructure-based crack propagation analyses can be used to get insights on pathways to achieve an optimal self-healing material system, ie, a design with the capability to trigger healing process but one which does not significantly lower the structural integrity of the original unfilled matrix material.

ACKNOWLEDGMENTS

This work was funded in part by IOP Self-Healing Materials (Agentschap NL, now Rijksdienst voor Ondernemend Nederland RVO) through project SHM01021 and in part by the European Union's Seventh Framework Programme (FP7) through the NMP SAMBA project (grant number 309849). We thank the IOP Self-Healing Materials and the Seventh European Framework Programme for their financial support of our research. We thank our collaborators Xun Zhang, Justyna Kulczyk-Malecka, and Ping Xiao at University of Manchester for providing the microstructure. We extend our sincere thanks to our collaborator Prof W. G. Sloof for his valuable support and interactive discussions.

NOMENCLATURE

T	effective traction
Δ	effective opening displacement
$\boldsymbol{t}$	traction vector
$\boldsymbol{\delta}$	cohesive crack opening displacement vector
t_n, t_s	cartesian components of traction vector
δ_n, δ_s	cartesian components of cohesive opening displacement vector
K	initial slope of cohesive law
σ_c	cohesive strength
G_c	fracture energy (toughness)
E	Young's modulus of the material
γ	non-dimensional mode mixity ratio
f_d	loading function
κ_d	damage history variable
g	effective traction-separation law
ω	damage variable
Δ_0	equivalent crack opening at onset of damage
Δ_f	equivalent crack opening at complete failure
$\delta_{n,0}, \delta_{s,0}$	crack opening at onset of damage for pure mode I and mode II respectively
$t_{n,c}, t_{s,c}$	cohesive strength for pure mode I and mode II respectively
$\delta_{n,f}, \delta_{s,f}$	crack opening at complete failure for pure mode I and mode II respectively
$\sigma_c^p, \sigma_c^m, \sigma_c^i$	cohesive (fracture) strength of particle, matrix and interface respectively
$\sigma_c^p, \sigma_c^m, \sigma_c^i$	fracture energy (toughness) of particle, matrix and interface respectively
E_p, E_m	Young's modulus of particle and matrix respectively
$\boldsymbol{\sigma^e}$	effective (or average) stress in the composite specimen
$\boldsymbol{\epsilon^e}$	effective strain in the composite specimen
σ_c^m	effective strength of a homogenous matrix specimen
ϵ_c^m	effective strain corresponding to the strength of a homogenous matrix specimen.

ORCID

Sathiskumar A. Ponnusami http://orcid.org/0000-0002-2143-8971

REFERENCES

1. Bergman SD, Wudl F. Mendable polymers. *J Mater Chem*. 2008;18(1):41-62.
2. Sloof WG, Pei R, McDonald SA, et al. Repeated crack healing in MAX-phase ceramics revealed by 4D in situ synchrotron X-ray tomographic microscopy. *Sci Rep*. 2016;6(1):23040.
3. Song GM, Pei YT, Sloof WG, Li SB, De Hosson JTM, van der Zwaag S. Oxidation-induced crack healing in Ti_3AlC_2 ceramics. *Scr Mater*. 2008;58(1):13-16.
4. Yıldırım G, Keskin ÖK, Keskin SB, Şahmaran M, Lachemi M. A review of intrinsic self-healing capability of engineered cementitious composites: recovery of transport and mechanical properties. *Constr Build Mater*. 2015;101:10-21.
5. Garcia SJ. Effect of polymer architecture on the intrinsic self-healing character of polymers. *Eur Polym J*. 2014;53: 118-125.
6. Sloof WG, Turteltaub S, Carabat AL, Derelioglu Z, Ponnusami SA, Song GM. Crack healing in yttria stabilized zirconia thermal barrier coatings. In: van der Zwaag S, Brinkman E, eds. *Self Healing Materials- Pioneering Research in the Netherlands*. Netherlands: IOS Press; 2015:219-227.
7. Ono M, Nakao W, Takahashi K, Ando K. Strength recovery of machined Al_2O_3/SiC composite ceramics by crack healing. *Fatigue Fract Eng Mater Struct*. 2007;30(12):1140-1148.
8. Pang JWC, Bond IP. 'Bleeding composites'—damage detection and self-repair using a biomimetic approach. *Compos Part A Appl Sci Manuf*. 2005;36(2):183-188.
9. Yoshioka S, Boatemaa L, van der Zwaag S, Nakao W, Sloof WG. On the use of TiC as high-temperature healing particles in alumina based composites. *J Eur Ceram Soc*. 2016;36(16):4155-4162.
10. Kanellopoulos A, Giannaros P, Palmer D, Kerr A, Al-Tabbaa A. Polymeric microcapsules with switchable mechanical properties for self-healing concrete: synthesis, characterisation and proof of concept. *Smart Mater Struct*. 2017;26(4):045025.
11. Hilloulin B, Tittelboom KV, Gruyaert E, Belie ND, Loukili A. Design of polymeric capsules for self-healing concrete. *Cement Concrete Comp*. 2015;55:298-307.
12. White SR, Sottos NR, Geubelle PH, et al. Autonomic healing of polymer composites. *Nature*. 2001;409(6822):794-797.
13. Kessler MR, Sottos NR, White SR. Self-healing structural composite materials. *Compos Part A Appl Sci Manuf*. 2003;34(8): 743-753.
14. Carabat AL, van der Zwaag S, Sloof WG. Creating a protective shell for reactive $MoSi_2$ particles in high-temperature ceramics. *J Am Ceram Soc*. 2015;98(8):2609-2616.
15. Kulczyk-Malecka J, Zhang X, Carr J, et al. Thermo-mechanical properties of SPS produced thermal barrier coatings containing pure and alloyed $MoSi_2$ particles. *J Eur Ceram Soc*. 2018;38: 4268-4275.
16. Ponnusami SA, Turteltaub S, van der Zwaag S. Cohesive-zone modelling of crack nucleation and propagation in particulate composites. *Eng Fract Mech*. 2015;149:170-190.
17. Ayyar A, Chawla N. Microstructure-based modeling of the influence of particle spatial distribution and fracture on crack growth in particle-reinforced composites. *Acta Mater*. 2007;55(18):6064-6073.
18. Ayyar A, Chawla N. Microstructure-based modeling of crack growth in particle reinforced composites. *Compos Sci Technol*. 2006;66(13):1980-1994.
19. Cannillo V, Manfredini T, Montorsi M, Siligardi C, Sola A. Microstructure-based modelling and experimental investigation of crack propagation in glass-alumina functionally graded materials. *J Eur Ceram Soc*. 2006;26(15):3067-3073.
20. Sozhamannan GG, Prabu SB, Paskaramoorthy R. Failures analysis of particle reinforced metal matrix composites by microstructure based models. *Mater Des*. 2010;31(8):3785-3790.
21. Qing H, Liu T. Micromechanical analysis of SiC/Al metal matrix composites: finite element modeling and damage simulation. *Int J Appl Mech*. 2015;07(02):1550023.
22. Qing H. Micromechanical study of influence of interface strength on mechanical properties of metal matrix composites under uniaxial and biaxial tensile loadings. *Comput Mater Sci*. 2014;89:102-113.
23. Li Y, Zhou M. Prediction of fracture toughness of ceramic composites as function of microstructure: I. Numerical simulations. *J Mech Phys Solids*. 2013;61(2):472-488.
24. Li Y, Zhou M. Prediction of fractures toughness of ceramic composites as function of microstructure: II. Analytical model. *J Mech Phys Solids*. 2013;61(2):489-503.
25. Mishnaevsky L, Derrien K, Baptiste D. Effect of microstructure of particle reinforced composites on the damage evolution: probabilistic and numerical analysis. *Compos Sci Technol*. 2004;64(12):1805-1818.
26. Williams JJ, Segurado J, LLorca J, Chawla N. Three dimensional (3D) microstructure-based modeling of interfacial decohesion in particle reinforced metal matrix composites. *Mater Sci Eng A*. 2012;557:113-118.
27. Zhang J, Ouyang Q, Guo Q, et al. 3D Microstructure-based finite element modeling of deformation and fracture of SiCp/Al composites. *Compos Sci Technol*. 2016;123:1-9.
28. Gilabert FA, Garoz D, Paepegem WV. Macro- and micro-modeling of crack propagation in encapsulation-based self-healing materials: application of XFEM and cohesive surface techniques. *Mater Des*. 2017;130:459-478.
29. Gilabert FA, Van Tittelboom K, Tsangouri E, Van Hemelrijck D, De Belie N, Van Paepegem W. Determination of strength and debonding energy of a glass-concrete interface for encapsulation-based self-healing concrete. *Cement Concrete Comp*. 2017;79:76-93.
30. Quayum MS, Zhuang X, Rabczuk T. Computational model generation and RVE design of self-healing concrete. *Frontiers Struc Civil Eng*. 2015;9(4):383-396.
31. Li W, Jiang Z, Yang Z, Yu H. Effective mechanical properties of self-healing cement matrices with microcapsules. *Mater Des*. 2016;95:422-430.
32. Lv L-Y, Zhang H, Schlangen E, Yang Z, Xing F. Experimental and numerical study of crack behaviour for capsule-based self-healing cementitious materials. *Constr Build Mater*. 2017;156:219-229.
33. Wang L, Shao F, Zhong XH, et al. Tailoring of self-healing thermal barrier coatings via finite element method. *Appl Surf Sci*. 2018;431:60-74. 5th Asian Conference on Heat Treatment and Surface Engineering.
34. Kulczyk-Malecka J, Zhang X, Carr J, et al. Influence of embedded $MoSi_2$ particles on the high temperature thermal conductivity of SPS produced yttria-stabilised zirconia model thermal barrier coatings. *Surf Coat Technol*. 2016;308: 31-39.
35. Ortiz M, Pandolfi A. Finite-deformation irreversible cohesive elements for three-dimensional crack-propagation analysis. *Int J Numer Meth Eng*. 1999;44(9):1267-1282.
36. Ponnusami SA, Krishnasamy J, Turteltaub S, van der Zwaag S. A cohesive-zone crack healing model for self-healing materials. *Int J Solids Struc*. 2018;134:249-263.
37. Schneibel JH, Sekhar JA. Microstructure and properties of $MoSi_2$-MoB and $MoSi_2$-Mo_5Si_3 molybdenum silicides. *Mater Sci Eng A*. 2003;340(1-2):204-211.

38. Selçuk A, Atkinson A. Strength and toughness of tape-cast yttria-stabilized zirconia. *J Am Ceram Soc*. 2004;83(8):2029-2035.
39. Adams JW, Ruh R, Mazdiyasni KS. Young's modulus, flexural strength, and fracture of yttria-stabilized zirconia versus temperature. *J Am Ceram Soc*. 2005;80(4):903-908.
40. Kondoh J, Shiota H, Kawachi K, Nakatani T. Yttria concentration dependence of tensile strength in yttria-stabilized zirconia. *J Alloy Compd*. 2004;365(1-2):253-258.
41. Schneibel JH, Kramer MJ, Ünal Ö, Wright RN. Processing and mechanical properties of a molybdenum silicide with the composition Mo-12Si-8.5B (at.%). *Intermetallics*. 2001;9(1):25-31.
42. Petrovic JJ. Mechanical behavior of $MoSi_2$ and $MoSi_2$ composites. *Mater Sci Eng A*. 1995;192-193:31-37.
43. Ponnusami SA, Turteltaub S, Zhang X, Xiao P. Modelling crack propagation in particle-dispersed self-healing thermal barrier coatings. In: van der Zwaag S, Brinkman E, eds. *Self Healing Materials- Pioneering Research in the Netherlands*. Netherlands: IOS Press; 2015:229-241.
44. Yang J-M, Jeng SM. Interface and mechanical behavior of $MoSi_2$-based composites. *J Mater Res*. 1991;6(03):505-513.

How to cite this article: Ponnusami SA, Krishnasamy J, Turteltaub S, van der Zwaag S. A micromechanical fracture analysis to investigate the effect of healing particles on the overall mechanical response of a self-healing particulate composite. *Fatigue Fract Eng Mater Struct*. 2019;42:533–545. https://doi.org/10.1111/ffe.12929